LES OF THE FLOW AROUND A CYLINDER OF FINITE HEIGHT

Jochen Fröhlich
Institut für Chemische Technik, Universität Karlsruhe
Kaiserstrasse 12, 76128 Karlsruhe, Germany
froehlich@ict.uni-karlsruhe.de

Wolfgang Rodi
Institut für Hydromechanik, Universität Karlsruhe
Kaiserstrasse 12, 76128 Karlsruhe, Germany,
rodi@uni-karlsruhe.de

ABSTRACT

The paper presents large eddy simulations of the flow around a surface–mounted circular cylinder at a Reynolds number of $Re = 43000$ of height $H = 2.5D$. In the first part, the different modelling parameters are discussed with respect to their influence on the computed results. One of the findings is that, on the relatively coarse grid employed, the dynamic model is deficient as it yields too large eddy viscosities. The results obtained with the Smagorinsky model are in fairly good agreement with measurements. In the second part of the paper these results are evaluated in detail and related to findings in the literature.

INTRODUCTION

The flow around bluff bodies such as wall-mounted cubes, cylinders, tube bundles, etc. has been attracting considerable interest due to its industrial relevance. Long bodies like cylinders of high aspect ratio typically lead to pronounced regular vortex shedding with the potential of creating resonances which in turn may provoke undesired flow features or even the failure of structures (Naudascher and Rockwell, 1994).

End effects alter the vortex shedding substantially and can mainly be grouped into those at free ends and those at a junction with a larger body or a wall. Both are encountered in case of a wall–mounted cylinder of finite height as sketched in Figure 1. Therefore, this flow is a prototype configuration which allows to study both effects and also the interaction between them. When reducing successively the height–to–diameter ratio H/D, the regular alternating vortex shedding being typical for a long cylindrical structure is, in an intermittent way, more and more replaced by symmetrically shed vortices in the range $H/D \approx 6$ to $H/D \approx 2$ (Kawamura *et al.*, 1984; Kappler, 2002). Vortex shedding is mostly suppressed for values around and below $H/D \approx 2$ (Okamoto and Yagita, 1973; Kappler, 2002). Compared to the case of an infinite cylinder, the number of influence parameters is substantially larger for cylinders of finite height. In addition to the Reynolds number Re and the free–stream turbulence level, the height–to–diameter ratio H/D and the thickness of the approaching boundary layer δ/H influence the flow as addressed by Kawamura *et al.* (1984) and subsequent publications. Due to the finite length of the body the average flow is, in contrast to the long cylinder, highly three–dimensional.

The interaction of different mechanisms of instability (like von Karman, Kelvin–Helmholtz, etc.) is a typical feature of bluff body flows. Here, the situation is further complicated by the end effects so that the detailed analysis of this flow is a substantial challenge. The aim of the present study is to perform large eddy simulations (LES) for this flow and to analyze its structure, and in particular the role and interaction of the various mechanisms.

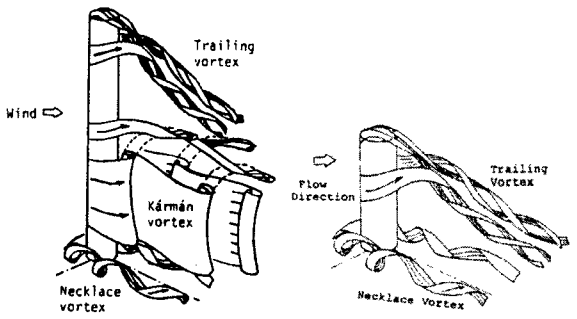

Figure 1: Sketches of the flow field around a cylinder of finite height from Kawamura *et al.* (1984). Left: situation if the cylinder is longer than the critical length for vortex shedding, right: the same if the cylinder is shorter.

CONFIGURATION INVESTIGATED

The flow around a circular cylinder of finite height studied here corresponds to an experiment performed by Kappler (2002) in a water tunnel. The Reynolds number was $Re = 43000$, based on the cylinder diameter and the free–stream velocity u_∞. For a long cylinder in uniform flow this value falls into in the sub–critical, more precisely into the "upper Transition in Shear Layer" regime $Re = 2 \cdot 10^4, \ldots, 2 \cdot 10^5$ (Zdravkovich, 1997). This regime exhibits only small changes with Reynolds number and is characterized by a laminar boundary layer along the cylinder wall, laminar separation, and transition to turbulence in the shear layer shortly after separation through a Kelvin–Helmholtz instability and further spanwise instabilities. This scenario requires low turbulence approach–flow. It is relevant for the present case, since in the experiment the turbulence level was $Tu = 2\%$, and indeed was observed in both, experiment and simulation. Note that the Reynolds number is fairly high for an LES since the boundary layer along the cylinder surface is very thin but needs to be resolved.

Different ratios H/D were investigated in the experi-

ment. Here, we select the case $H/D = 2.5$ so that according to the above discussion only a small amount of regular vortex shedding is to be expected. The boundary layer thickness of the approaching flow was $\delta/H = 0.1$ which is small and does not correspond to applications in building aerodynamics. The width of the tunnel was $7D$ and the height $5D$ introducing a blockage of 7.3%.

The available experimental data result from two–component LDA measurements in different horizontal and vertical planes. The measured quantities are the streamwise velocity component together with a second component, depending on the orientation of the laser beam, and in each case the corresponding fluctuations.

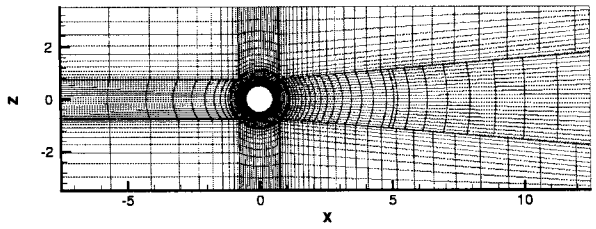

Figure 2: Two–dimensional cut in wall–parallel direction through grid G2. Only every 4th point is plotted (the complete grid has no hanging nodes).

NUMERICAL METHOD AND LES MODELLING

The simulations have been performed with the code LESOCC2 which is a successor of the code LESOCC (Breuer and Rodi, 1996) and solves the incompressible Navier–Stokes equations on curvilinear block–structured grids. A collocated Finite–Volume discretization with second order central schemes for convection and diffusion terms is employed. Temporal discretization is performed with a three–stage Runge–Kutta scheme solving the pressure–correction equation in the last stage only.

Table 1 provides an overview over the simulations performed. Two subgrid–scale models have been employed in these computations. One is the Smagorinsky model with van Driest damping based on the length scale

$$l = C_s \Delta (1 - \exp(-y^+/25)^3)^{1/2} \qquad (1)$$

with $\Delta = (Vol)^{1/3}$ and Vol the volume of a computational cell. The constant is chosen as $C_s = 0.1$. The second is the dynamic model of Germano *et al.* (1991), here employed with least squares averaging and three–dimensional test filtering. The eddy viscosity $\nu_t = l^2|S|$, with S being the resolved strain–rate tensor, is regularized by relaxing $l = C_s\Delta$ in time and imposing $0 \leq \nu_t \leq 100\nu$ where ν is the molecular viscosity.

The width and the height of the computational domain were selected to be the same as in the experiment, hence introducing the same blockage. With the base of the cylinder located at the origin of the coordinate system and x, y, z representing the streamwise, wall–normal and lateral direction, respectively, this yields $y/D = 0, \ldots, 5$ and $z/D = -3.5, \ldots, 3.5$ (see Figure 2). The outflow boundary is located at $x/D = 12.5$ where a convective boundary condition was imposed. The upstream boundary condition is located at $x/D = -7.5$ where a constant velocity $u = u_\infty$ was imposed. Such a condition has been used successfully already for the simulation of flows around long cylinders (Fröhlich *et al.*, 1998) and is justified here for the case of a very thin bottom–wall boundary layer. The boundary condition on the cylinder surface was a no–slip condition in all computations. The conditions at the top wall and at the sidewalls were free–slip conditions.

Table 1: Overwiew over the simulations performed. The different columns assemble infromation on the number of grid points, the bottom–wall boundary condition, the subgrid–scale modelling, the averaging time t_a, and the mean drag coefficient.

Run	grid	bottom	SGS	t_a	C_D
G1SS	$1.0\,10^6$	slip	SM	155	0.32
G2SS	$6.4\,10^6$	slip	SM	123	0.88
G2WS	$6.4\,10^6$	WW	SM	100	0.88
G2WD	$6.4\,10^6$	WW	DSM	83	0.6

The first two computations, G1SS and G2SS, employed a frictionless ground plate which is equivalent to imposing a symmetry plane. Consequently, no boundary layer develops along the bottom wall, but the flow around the free end can be investigated (Fröhlich *et al.*, 2002). Two grids were used, a coarse grid (G1) with 1 Mio. points and a finer grid (G2) with 6.4 Mio. points partitioned into 24 blocks. The latter is displayed in Figure 2. The same grid was then used imposing a solid ground plate with friction using the Werner and Wengle (1993) wall function. With this condition a small boundary layer develops along the bottom wall. It has been compared to measurements in the empty tunnel and found to exhibit similar profiles of mean and fluctuating streamwise velocity. In another computation the impact of the subgrid–scale model was investigated by employing the dynamic model. The time step in all simulations was adjusted instantaneously according to the stability criterion of the time scheme which yielded values around $10^{-3}D/u_\infty$.

RESULTS

The impact of the different numerical and modelling parameters on the result will be discussed first by means of averaged quantities. Figure 3 compares streamwise mean velocity and related fluctuations for the different runs to the experimental data. Figures 4 and 5 show average streamlines and fluctuations for G2SS and G2WS in comparison with those from the experiment. All quantities are given in units of D for lengths, u_∞ for velocities, and D/u_∞ for time.

Table 1 reports the mean drag coefficient $C_D = f_x/0.5\rho u_\infty^2 LD$ which can serve as a first criterion for assessment. The temporal evolution of lift and drag force f_z and f_x, respectively, is depicted in Figure 9 below for run G2WS. These include both pressure and viscous forces. Experimental values for C_D have been obtained either by direct measurement or by integration of the pressure over the surface (since the viscous contribution is comparatively small). It is generally observed that C_D decreases when reducing H/D due to the intrusion of the flow over the top into the wake. On the other hand, the drag increases with reduced boundary layer thickness δ/H and also depends on the free stream turbulence level and the blockage Bl, similar to the long cylinder. Hence, for a particular set–up it is hard to find exactly matching conditions in the literature (in the companion experiment of Kappler (2002) no pressures or forces were measured). Experimental values

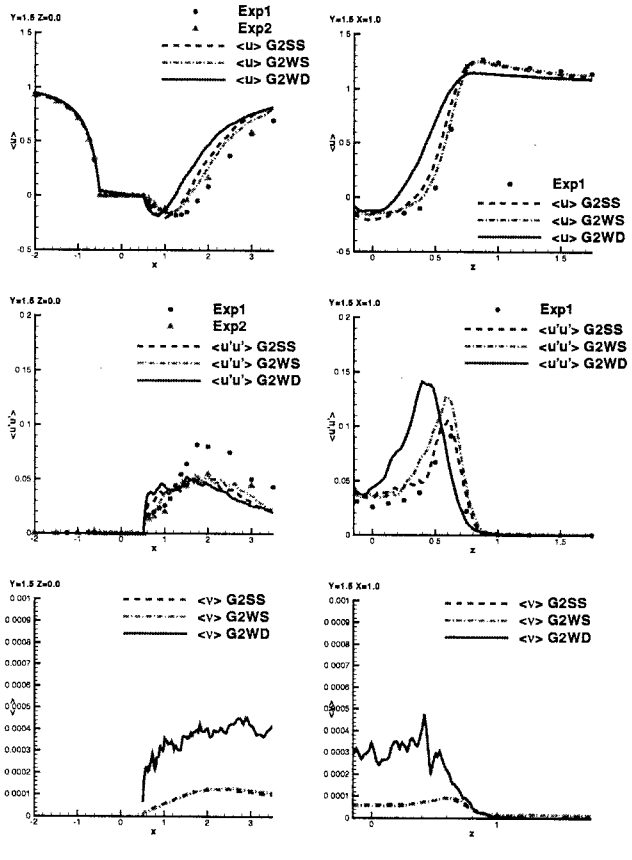

Figure 3: Average quantities along lines at an elevation $y/D = 1.5$ above the bottom wall. Left: in the center plane with $z/D = 0$. Right: in lateral direction at $x/D = 1$. Streamwise mean velocity (top) and corresponding fluctuations (middle) and average turbulent viscosity (bottom). Lines: LES, symbols: experimental data from Kappler (2002).

from situations similar to the present one are $C_D = 0.78$ ($H/D = 2, \delta/H = 0.1, BL = 0.88\%$, (Kawamura *et al.*, 1984)) and $C_D = 0.73$ ($H/D = 2, \delta/H = 0.1, BL = 1.3\%$, (Okamoto and Sunabashiri, 1992)) in the same Reynolds number regime. The fairly large influence of the blockage ratio can be appreciated by reference to the value $C_D = 1.22$ ($H/D = 2, \delta/H = 0.1, BL = 11.2\%$, (Baban and So, 1991)). In light of these data the present value of $C_D = 0.88$ obtained by simulation G2WS for a blockage ratio of 7.3% is in good agreement with the literature.

Influence of the grid

A comparison of runs G1SS and G2SS in Table 1 shows the effect of insufficient resolution. Streamline plots (not displayed here) reveal that the shear layers separating from the cylinder are shifted towards the x–axis due to delayed separation, the wake narrows and as a consequence the drag is substantially reduced when a coarser grid is used. The Smagorinsky model, when employed with grid G2, yields a fairly good match with the experiment as shown by the curves in Figure 3 and the plots in Figures 4 and 5. This is improved even further when friction at the bottom wall is accounted for.

Influence of the subgrid–scale model

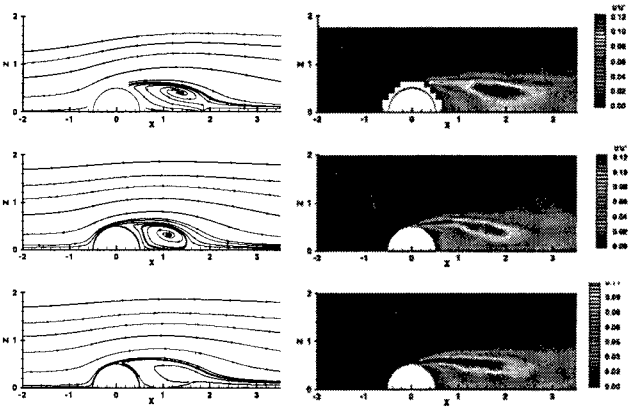

Figure 4: Average streamlines at $y/D = 1.5$ (left) and $\langle u'u' \rangle$ in the same plane (right). The colour scale ranges from 0 to 0.12. Top: experiment, middle: run G2SS, bottom: run G2WS.

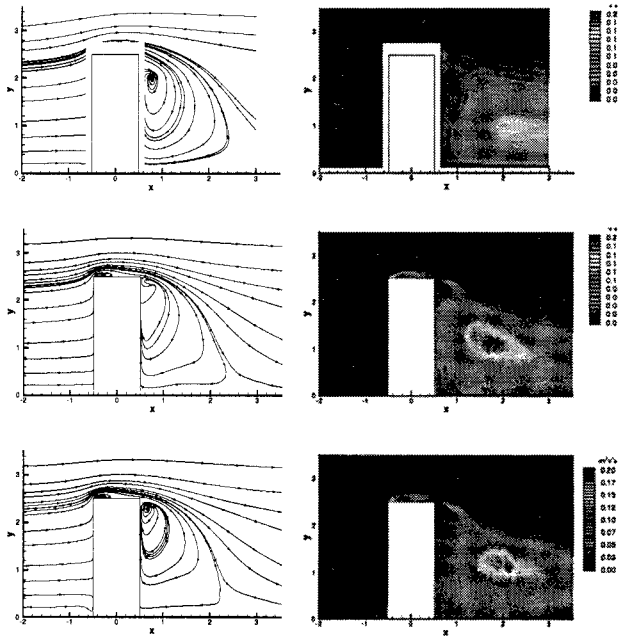

Figure 5: Average streamlines (left) and vertical fluctuations $\langle v'v' \rangle$ (right) in the centerplane $z/D = 0$. The colour scale ranges from 0 to 0.2. Top: experiment, middle: run G2SS, bottom: run G2WS.

The Reynolds number is high and the grid G2 in the upstream part and along the cylinder wall is still relatively coarse for an LES. When switching to the dynamic model, the test filter operation projects the velocity onto an even coarser grid and as a consequence excessive eddy viscosity in the shear layer and the near wake is produced. In the locations considered in Figure 3, e.g., it is by about a factor of 4 larger. This yields a shift of the shear layers towards the center plane and hence a reduction of the drag, similar to the impact of the coarse grid but not as strong (see Table 1 and pictures of Figure 3).

Since it is known from LES of long cylinders that the resolution in direction of the cylinder axis is important for the representation of the shear layer instability (Fröhlich

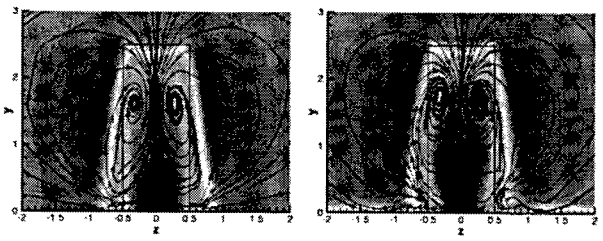

Figure 6: Impact of the bottom wall boundary condition on the wake. Left: average streamwise velocity and streamtraces at $x = 1$ with slip condition (run G2SS). Right: the same data with a solid wall (run G2WS).

et al., 1998; Kravchenko and Moin, 2000) the grid G2 has been refined in wall normal direction. Furthermore, the discretization in streamwise and spanwise direction was refined. This improved the discretization of the wall boundary layer upstream and downstream of the cylinder. A computation with this grid, G3, and the dynamic model is currently under way but has not yet accumulated sufficient averaging. We can however state that with this grid the dynamic model yields a level of viscosity comparable to the runs G2SS and G2WS.

Influence of the bottom wall boundary condition

We now address the influence of the bottom wall boundary condition which can be assessed by comparison of runs G2SS and G2WS. The wall boundary layer is thin, with $\delta/H \approx 0.1$ so that the effect of accounting for its development is small. In particular, the flow upstream of the cylinder is little affected as evidenced by the low position of the saddle point on the stagnation line and the thin horseshoe vortex shown in Figures 10 and 11 below. However, in the rear the bottom boundary condition can have some influence the evolution of the shed vortices. In order to investigate this, cuts normal to the streamwise axis at $x/D = 1$ are displayed in Figure 6 showing that the wake narrows somewhat near the lower boundary if a boundary layer is allowed to develop. Also, accounting for the bottom boundary layer appears to improve somewhat the recirculation pattern behind the cylinder (Figure 5).

Instantaneous flow

An impression of the instantaneous flow is given by Figure 7 from G2WS displaying an iso–surface of the normalized instantaneous deviation of the pressure from the average $\tilde{p}' = (p - \langle p \rangle)/(\rho u_\infty^2)$. This visualization of the flow structure was complemented by further views and animations upon which the following comments are based. They show the separation at the sharp front corner of the cylinder top to be fairly regular, exhibiting lateral vortex rollers which interwind and merge upon travelling downstream along the roof. Around the rear of the top end the separation process is highly complex and very irregular due to the curved trailing edge and the separation at the sidewalls so that organized motion can hardly be detected. Near the top, the separation along the cylinder shaft is similarly influenced by the flow over the free end but becomes more regular further down towards the bottom wall. There, the separation takes place in a more coherent way and larger vortices with their axis parallel to the cylinder axis are formed. In the experiment no regular vortex shedding was detected near the top end and regular alternating shedding near the bottom surface for all

Figure 7: Instantaneous flow structures obtained from G2WS Iso–surface of the instantaneous pressure deviation, $\tilde{p}' = -0.05$, viewed from the top and at an oblique angle from the rear.

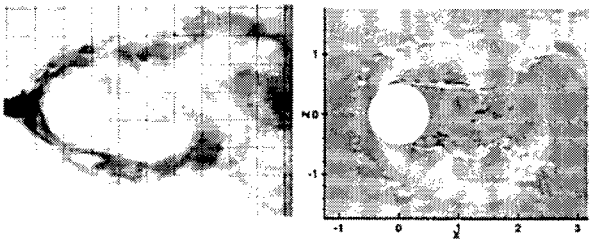

Figure 8: Instantaneous picture of vortex shedding close to the ground plate. Left: visualization by means of a trace in the experiment Kappler (2002), right: instantaneous $u-$velocity in the wall–adjacent cell from run G2WS.

aspect ratios (Kappler, 2002). For $H/D = 2.5$, symmetrical vortex shedding occasionally occurred near the bottom in rare events. Figure 8 presents a tracer photograph near the bottom plate from the experiment and a plot from G2WS showing the instantaneous $u-$velocity at an instant with alternating vortex shedding.

Further downstream in the wake the shed vortices increase in size and become smoother. Highly distorted Karman vortices are visible in Figure 7. They are bent inwards and backwards due to the downward motion behind the cylinder visible in the streamline pictures of Figure 5. Comparison with the sketch in Figure 1 shows that, as observed in the experiments, the present ratio $H/D = 2.5$ is too small for regular Karman vortices parallel to the cylinder axis to appear. Such vortex shedding takes place only for longer cylinders.

The irregular separation and shedding processes produce relatively irregular forces on the cylinder. This is illustrated in Figure 9 by showing the temporal evolution of the instantaneous lift and drag forces for G2WS (corresponding

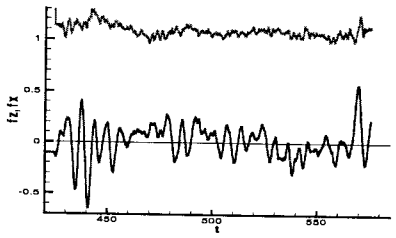

Figure 9: Lift force f_z (lower curve) and drag force f_x (upper curve) for run G2WS.

pictures for the other runs look similar, but with different average values of the coefficients). While a dominant frequency f with a Strouhal number of about $St = fD/u_\infty = 0.16$ can be discerned, the lift coefficient exhibits an irregularly changing amplitude and can have an average different from zero over a certain number of shedding periods. This is a demanding situation and requires long averaging times making the computations very expensive.

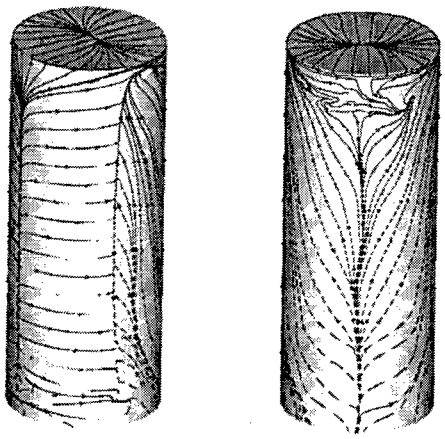

Figure 10: Surface streamlines from run G2WS. Left: oblique view with flow from left to right. Right: rear view.

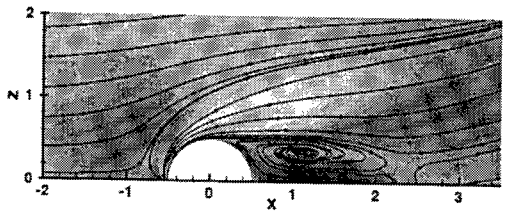

Figure 11: Average streamlines in the wall–adjacent cell along the bottom wall from run G2WS. The color scale represents the average streamwise velocity component.

Average flow

The average flow is now discussed focusing on the results of run G2WS which previously were found to be in best agreement with the experiment. Figures 4 and 5 show streamlines from the LES and compare them to the ones obtained from G2SS and the corresponding experiment (there are no experimental streamlines close to solid walls since LDA measurements were not possible there). A separation bubble can be observed on the top with reattachment around the middle of the roof as visible in the surface streamline pictures in Figure 10 below. Behind the cylinder, the streamlines in the center plane exhibit a large recirculation region (see Figure 5) with the center of the vortex around $x \approx 0.8, y \approx 2$ in the experiment and somewhat higher and closer to the cylinder in the LES. However, the length of the recirculation region in simulation and experiment can be seen to be similar. Figures 4 and 5 also show calculated contours of velocity fluctuations in comparison with the experimental contours (u–fluctuations in a horizontal plane at $y/D = 1.5$ in Figure 4 and v–fluctuations in the vertical symmetry plane in Figure 5). Again the agreement is fairly good.

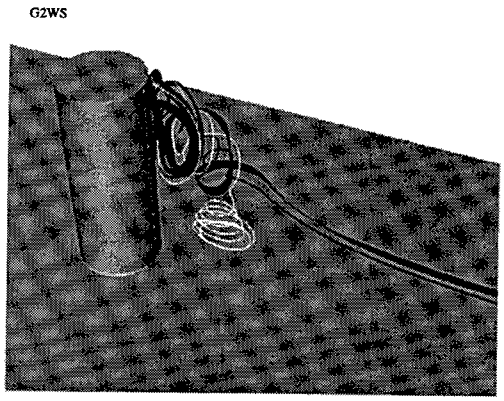

Figure 12: Visualization of the vortex structure behind the cylinder (run G2WS).

Figure 10 and 11 show streamlines in wall–adjacent cells along the cylinder surface and the bottom wall, respectively. The stagnation line running from $y/D = 0.2$ to $y/D = 2.1$ is clearly visible in the left oblique view of Figure 10. Near the bottom a saddle point exists at $y/D = 0.2$ resulting from the oncoming boundary layer. Along the shaft there is a slight upward motion, but on the side the lines remain fairly horizontal. Near the upper end the stagnation line splits up into a fan of streamlines due to the end effect. The separation line along the side wall is also visible. It is located at a fairly constant angle of 80 degrees from the stagnation line along the shaft, but curves towards the rear for $(H - y)/D < 1D$. Upstream of the curved separation line a pressure minimum with $c_P = (\langle p \rangle - p_\infty)/0.5\rho u_\infty^2) = -1.2$ is located at $y/D = 2.25$ and an angle of 70 degrees from the stagnation line. This observation corresponds to measurements of Uematsu and Yamada (1994) and Kawamura *et al.* (1984).

The recirculating flow in the rear of the separation line exhibits a substantial upward motion as was to be expected from Figure 5. At $y/D \approx 2.3$ and $z/D \approx \pm 0.3$ a focus is visible in the right picture resulting from the upward rear motion and the counteracting downward motion in the center plane. On the roof, the reattachment of the flow mentioned above is observed in the middle of the roof. In the companion experiment no oil flow pictures were taken, but the behaviour just described corresponds qualitatively to the pictures taken by Hölscher (1993), which can be found in Majumdar and Rodi (1989), albeit for a cylinder placed in a much thicker boundary layer ($\delta/H = 2.54$).

The average recirculation observed in wall–parallel planes (Figure 4) also induces a footprint on a surface, now

the bottom plane, as shown in Figure 11. This figure also indicates a small horseshoe vortex forming in front of the cylinder and bending around it.

The foci on the rear of the cylinder close to the top in the right part of Figure 10 are the footprints of two tip vortices which separate from the cylinder's free end and reach down into the wake (see Figure 1). One of them was visualized by means of a stream ribbon as displayed in Figure 12. Its motion is somewhat irregular near the cylinder as it is caught in the horizontal vortex at $x \approx 0.8$, $y \approx 2$ discussed in relation to Figure 5 above. At a height of about $y/D \approx 1$ the stream ribbon leaves this vortex and stretches downstream until the exit of the domain, still spiralling but at a much lower pace. Two further streamtraces have also been introduced in close vicinity for clarification. The black one spirals in the interior of the ribbon's traces and indeed resembles the tip vortex in Figure 1. The second, white one, remains further outward close to the ribbon but continues down to the bottom plate. The tip vortices, already displaced downward, can also be seen in Figure 6

The results of Figure 12, as well as of 4 and 5, suggest the presence of an arch–type vortex similar to the one observed in the flow around a surface–mounted cube (Martinuzzi and Tropea, 1993). This vortex, which is a feature of the average, not the instantaneous flow, should possibly be included in sketches like the ones reproduced in Figure 1.

CONCLUSIONS

We have presented several LES of the flow around a surface–mounted cylinder of finite height. A detailed comparison to a companion experiment has shown that the results obtained with the Smagorinsky subgrid–scale model capture the main features of this complex flow quite well. It was found that with the dynamic model, a finer grid is necessary which has been generated and is used in further simulations. The results show the details of the complicated vortex shedding process where separation from the sidewalls and the roof of the cylinder interact closely. The relatively small height of the cylinder does not allow teh development of 2D Karman vortices, but these are bent and distorted as they travel along the wake. The average flow is shown to exhibit an arch–type vortex behind the cylinder as observed in the flow around a wall–mounted cube. This has not previously been reported in the literature on the subject.

Acknowledgments: The authors acknowledge funding through the German Research Foundation within the DFG-CNRS programme 'Numerical Flow Simulation', SFB 606, and through a travel grant. The computing time was kindly provided by the computing center of FZK Karlsruhe. The authors also thank M. Kappler for providing his experimental data.

REFERENCES

Baban, F. and So, R. (1991). "Aspect ratio effect on flow-induced forces on circular cylinders in a cross flow", *Exp. in Fluids*, **10**, 313–321.

Breuer, M. and Rodi, W. (1996). "Large eddy simulation of complex turbulent flows of practical interest", In E. Hirschel, editor, *Flow simulation with high performance computers II*, volume 52 of *Notes on Numerical Fluid Mechanics*, pages 258–274. Vieweg, Braunschweig.

Fröhlich, J., Rodi, W., Kessler, P., Parpais, S., Bertoglio, J., and Laurence, D. (1998). "Large eddy simulation of flow around circular cylinders on structured and unstructured grids", In E. Hirschel, editor, *Numerical Flow Simulation I*, volume 66 of *Notes on Numerical Fluid Mechanics*, pages 319–338. Vieweg.

Fröhlich, J., Rodi, W., Dewan, A., and Fontes, J. (2002). "Large eddy simulation of flow around the free end of a circular cylinder", In E. Hirschel, editor, *Numerical Flow Simulation III*, volume 82 of *Notes on Numerical Fluid Mechanics*, pages 191–202. Springer.

Germano, M., Piomelli, U., Moin, P., and Cabot, W. (1991). "A dynamic subgrid–scale eddy viscosity model", *Phys. Fluids A*, **3**, 1760–1765.

Hölscher, N. (1993). "Ein multivariater Ansatz für die aerodynamische Übertragungsfunktion der Winddrücke in atmosphärischer Grenzschichtströmung", Ph.D. thesis, Ruhr–Universität Bochum.

Kappler, M. (2002). "Experimentelle Untersuchung der Umströmung von Kreiszylinder mit ausgeprägt dreidimensionalen Effekten". Ph.D. thesis, Institute for Hydromechanics, University of Karlsruhe.

Kawamura, T., Hiwada, M., Hibino, T., Mabuchi, I., and Kamuda, M. (1984). "Flow around a finite circular cylinder on a flat plate", *Bulletin of the JSME*, **27**(232), 2142–2151.

Kravchenko, A. G. and Moin, P. (2000). "Numerical studies of flow over a circular cylinder at $Re_D = 3900$" *Phys. Fluids*, **12**, 403–417.

Majumdar, S. and Rodi, W. (1989). "Three-dimensional computation of flow past cylindrical structures and model cooling towers", *Building and Environment*, **24**(1), 3–22.

Martinuzzi, R. and Tropea, C. (1993). "The flow around a surface–mounted prismatic obstacle placed in a fully developed channel flow" *J. Fluid Eng.*, **115**, 85–92.

Naudascher, E. and Rockwell, D. (1994). "Flow-induced vibrations: An engineering guide", IAHR Hydraulic Structures Design Manuals. Balkema Publishers, Rotterdam.

Okamoto, S. and Sunabashiri, Y. (1992). "Vortex shedding from a circular cylinder of finite length placed on a ground plane", *J. Fluids Eng*, **114**, 512–521.

Okamoto, T. and Yagita, M. (1973). "The experimental investigation on the flow past a circular cylinder of finite length placed mormal to the plane surface in a uniform stream", *Bulletin of the JSME*, **16**(95), 805–814.

Uematsu, Y. and Yamada, M. (1994). "Aerodynamic forces on circular cylinders of finite height", *J. Wind Eng. and Ind. Aerodyn.*, **51**, 249–265.

Werner, H. and Wengle, H. (1993). "Large–Eddy Simulation of turbulent flow over and around a cube in a plane channel", In F. Durst, R. Friedrich, B. Launder, F. Schmidt, U. Schumann, and J. Whitelaw, editors, *Selected Papers from the 8th Symposium on Turbulent Shear Flows*, pages 155–168. Springer.

Zdravkovich, M. (1997). "Flow Around Circular Cylinders", Oxford University Press.